A nonsmooth Newton multigrid method for a hybrid, shallow model of marine ice sheets

Guillaume Jouvet, Ed Bueler, Carsten Gräser, and Ralf Kornhuber

Abstract. The time evolution of ice sheets and ice shelves is model by combining a shallow lubrication approximation for shear deformation with the shallow shelf approximation for basal sliding, along with the mass conservation principle. At each time step two p-Laplace problems and one transport problem are solved. Both p-Laplace problems are formulated as minimisation problems. They are approximated by a finite element truncated nonsmooth Newton multigrid method. As an illustration, we compute the steady state shape of an idealized ice sheet/shelf system.

1. Introduction

Because of questions related to sea level rise [**VA07**], the literature on modeling of ice sheets and ice shelves has expanded in recent years [**DPF11, DGDF$^+$09, GHS09, PHDBDS06, VP05, WMH$^+$11**]. Special attention has been given to the grounding lines between ice sheets and ice shelves because they mostly control the stability of such marine ice sheets [**Sch07**]. Indeed, small perturbations of thermal state or climatic mass balance might lead the grounding line to move substantially, causing considerable changes to the geometry of the entire ice mass. The design of reliable models and fast numerical schemes is, therefore, important for understanding the evolution of marine ice sheets.

Ice is usually modelled as an incompressible non-Newtonian fluid, in a nonlinear Stokes problem [**GB09**], but the small aspect ratio of ice sheets can yield substantial simplifications of the stress balance. The vertical shear component is dominant in the majority of shallow ice sheets, giving a lubrication-type flow, while longitudinal components dominate in shallow ice shelves yielding a "plug" or membrane-type flow [**WMH$^+$11**]. However, at the grounding line both regimes are significant. The change of regime generally occurs within a few-kilometer zone of nested boundary layers [**Sch11**].

One can distinguish two kinds of marine ice sheet models. The first uses separate equations for the ice sheet and ice shelf, with an explicit evolution of the grounding line [**DPF11, Sch07**]. In two dimensions, such models are usually implemented with a moving grid such that the grounding line is one point of the mesh.

The first author was supported by the Swiss National Science Foundation (project 133349) and the Deutsche Forschungsgemeinschaft (project KL 1806 5-1).

The second author is supported by the NASA (grant NNX09AJ38G).

Unfortunately, in three dimensions, moving the mesh to follow the grounding line, a curve along the bedrock, is a harder task. Such two-mode models need to be connected by a continuity boundary condition at the grounding line.

The current paper adopts a second strategy. We use a unified model for both the ice sheet and shelf. The grounding line has an implicit description, namely the flotation criterion. We use an adaptive grid to deal with the sharp changes in flow regime close to the grounding line. Our model also derives the shape and evolution of grounded ice sheet margins from the same combination of equations, but in a parameter range where basal resistance dominates. Our results are for two-dimensional (plane) flows only; the three-dimensional case is in preparation.

2. Model

Let $\Omega \subset \mathbb{R}$ be the maximum horizontal extent of a two-dimensional ice sheet and $[0, T]$ be a time interval, with $T > 0$. We assume a fixed bedrock elevation function $z = b(x)$ in Ω. We denote by $l(x, t)$ and $s(x, t)$ the elevation of the lower and upper ice surfaces, respectively; $l = b$ where ice is grounded and $l > b$ where ice is floating (Fig. 1). The ice thickness is $h = s - l$, and $h \geq 0$ on Ω. Where the bedrock elevation b is above sea level $z = 0$, $h = 0$ is allowed. The functions s, l and h are continuous on Ω, and cliffs are allowed only at the boundary of Ω.

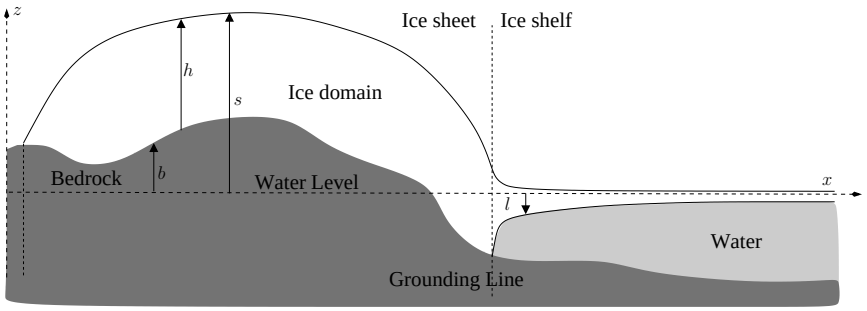

FIGURE 1. Notation for a two-dimensional ice sheet/shelf system.

Let ρ_i and ρ_w denote the densities of ice and water, respectively. Archimedes's principle for flotation implicitly determines the grounding line, so that the lower surface elevation is determined from other fields [**PSP$^+$12, WMH$^+$11**]:

$$l = \max\left\{b, -\frac{\rho_i}{\rho_w} h\right\}. \tag{2.1}$$

The grounding line is the abscissa where the maximum in (2.1) switches.

Following [**BB09, WMH$^+$11**], the ice flow is described by superposing velocity from the isothermal shallow ice approximation (SIA) model [**GB09**] that accounts for the vertical shear, and from the shallow shelf approximation (SSA) model [**Sch06a**] that accounts for the longitudinal stresses and basal friction (where grounded).

2.1. The shallow ice approximation. The isothermal SIA stress balance combines with mass conservation to give a single partial differential equation (PDE) for the ice thickness h [**GB09**]. Let $\Gamma = 2A(\rho_i g)^{p-1}/(p+1) > 0$, where $A > 0$

is the constant ice softness, $p = n_{\text{Glen}} + 1$ where the Glen flow law exponent has standard value $n_{\text{Glen}} = 3$ [**GB09**], and g the acceleration of gravity. The PDE is

$$\frac{\partial h}{\partial t} - \Gamma \frac{\partial}{\partial x}\left(h^{p+1} \left| \frac{\partial h}{\partial x} + \frac{\partial l}{\partial x} \right|^{p-2} \left(\frac{\partial h}{\partial x} + \frac{\partial l}{\partial x} \right) \right) + \frac{\partial}{\partial x}(hu) = a, \qquad \text{if } h > 0, \tag{2.2}$$

$$h = 0, \quad \text{otherwise.} \tag{2.3}$$

Here u is the basal sliding (defined later by the SSA model) and $a(x)$ is the climatic mass balance (accumulation and ablation). Equations (2.2), (2.3) should be interpreted as an obstacle problem that incorporates the free-boundary constraint $h \geq 0$ [**CDD$^+$02, JB**], however. The variational inequality form is

$$\begin{aligned} \int_\Omega \frac{\partial h}{\partial t}(v-h) + \Gamma \int_\Omega h^{p+1} \left| \frac{\partial h}{\partial x} + \frac{\partial l}{\partial x} \right|^{p-2} \left(\frac{\partial h}{\partial x} + \frac{\partial l}{\partial x} \right) \frac{\partial}{\partial x}(v-h) \\ + \int_\Omega \frac{\partial}{\partial x}(h\,u)\,(v-h) \geq \int_\Omega a(v-h), \end{aligned} \tag{2.4}$$

where $v \geq 0$ are test functions. The grounded ice sheet margin, the time-dependent free boundary of the ice domain $\{h > 0\}$, comes from solving (2.4).

2.2. The shallow shelf approximation. In this section, we describe the model which determines u in (2.4). The velocity u solves on the restricted ice domain $\{x \in \Omega,\ h(x) > 0\}$ the SSA equation [**Sch06a**]:

$$-2A^{1-q}\frac{\partial}{\partial x}\left(h \left| \frac{\partial u}{\partial x} \right|^{q-2} \frac{\partial u}{\partial x} \right) + C|u|^{m-1}u \times \mathbf{1}_{G(h)} = -\rho_i g h \frac{\partial s}{\partial x}, \quad \text{if } |u| > 0, \tag{2.5}$$

$$u = 0, \qquad \text{else,} \tag{2.6}$$

where $q = p/(p-1) \in (1,2)$ is the conjugate exponent to p and $m \geq 0$, $C \geq 0$ are given parameters. We denote the grounded set

$$G(h) := \{x \in \Omega,\, b(x) + (\rho_i/\rho_w)h(x) > 0\} \tag{2.7}$$

so that $\mathbf{1}_{G(h)}$ in (2.5) is equal to one in the grounded part and zero otherwise. Physically, the first term in (2.5) represents longitudinal stress gradients while the second term represents basal friction. The right-hand-side represents the gravitational forces in the form called the "driving stress" [**GB09**]. The $m = 0$ case is a Coulomb-type or "plastic till" friction law [**Sch06b, Sch06a, Sch09**]. On the boundary of $\{h > 0\}$, we have either a stress-free condition if the margin is grounded or a water-ice balance stress condition if the margin is floating, i.e. at the calving front. In both cases, the condition is:

$$2A^{1-q}h \left| \frac{\partial u}{\partial x} \right|^{q-2} \frac{\partial u}{\partial x} = \frac{1}{2}\left(1 - \frac{\rho_i}{\rho_w} \right) \rho_i g h^2 := F. \tag{2.8}$$

By extending u by zero where $h = 0$, equation (2.5) with boundary condition (2.8) is reformulated as the variational inequality [**Sch06a**]:

$$\begin{aligned} 2A^{1-q}\int_\Omega h \left| \frac{\partial u}{\partial x} \right|^{q-2} \frac{\partial u}{\partial x}\frac{\partial}{\partial x}(v-u) + \frac{C}{m+1}\int_{G(h)} (|v|^{m+1} - |u|^{m+1}) \\ + \rho_i g \int_\Omega h \frac{\partial s}{\partial x}(v-u) - \int_{\partial\Omega} F(v-u) \geq 0, \end{aligned} \tag{2.9}$$

where v is a test function. When $m > 0$, inequality (2.9) can be actually rewritten as a variational equality. Like (2.4), variational inequality (2.9) is attractive since it does not involve the boundary of the ice domain $\{h > 0\}$.

3. Approximations

3.1. Discretization in time. Variational inequality (2.4) derives from a nonlinear diffusion-advection equation (2.2). It is expected to be advection-dominated where floating and diffusion-dominated where grounded. Operator splitting techniques [**Glo03**, chapter 2] for solving (2.4) are used to decouple the advection and diffusion operators. This first-order splitting corresponds to first solving without the diffusion and source terms, and then solving without advection.

Let $N > 0$ and suppose $[t_0, ..., t_{N+1}]$ is a time discretization of $[0, T]$ with time steps $\tau_n = t_{n+1} - t_n, n = 0, 1, ..., N$. Denote by h_n an approximation of $h(t_n)$. Assuming h_n is known for some n, the following three-step scheme describes how to compute h_{n+1}.

I. Find u_n that minimizes:

$$\mathcal{J}_{SSA}(v) := \frac{2A^{1-q}}{q} \int_\Omega h_n \left| \frac{\partial v}{\partial x} \right|^q + \frac{C}{m+1} \int_{G(h_n)} |v|^{m+1} + \rho_i g \int_\Omega h_n \frac{\partial s_n}{\partial x} v - \int_{\partial\Omega} F v,$$

where $s_n = l_n + h_n$ and l_n is computed from (2.1) using h_n.

II. Find $h_{n+\frac{1}{2}}$, the solution at time t_{n+1} of the advection problem:

$$\begin{cases} \dfrac{\partial h}{\partial t} + \dfrac{\partial}{\partial x}(h u_n) & = 0, \qquad \text{on} \quad (t_n, t_{n+1}). \\ h(t_n) & = h_n, \end{cases}$$

III. Find $h_{n+1} \geq 0$ that minimizes over all $v \geq 0$:

$$\mathcal{J}_{SIA}(v) := \frac{1}{2\tau_n} \int_\Omega v^2 + \frac{\Gamma}{p} \int_\Omega (h_{n+\frac{1}{2}})^{p+2} \left| \frac{\partial v}{\partial x} + \frac{\partial l_{n+\frac{1}{2}}}{\partial x} \right|^p - \int_\Omega \left(\frac{h_{n+\frac{1}{2}}}{\tau_n} + a \right) v,$$

where $l_{n+\frac{1}{2}}$ is computed from (2.1) using $h_{n+\frac{1}{2}}$.

If $G(h_n)$ has a positive measure then one can show that the functional $\mathcal{J}_{SSA}$ is strictly convex and strongly-continuous in $W^{1,q}(\Omega)$ and therefore lower-semi-continuous [**Sch06b, Sch09**]. However, coerciveness in the $m > 0$ case would require h_n to be uniformly lower-bounded by a positive constant. The case $m = 0$, namely Coulomb friction, requires more hypotheses [**Sch09**]. As a consequence the well-posedness of the minimisation problem related to $\mathcal{J}_{SSA}$ is not guaranteed since h_n might tend to zero. One can show that $\mathcal{J}_{SIA}$ is strictly convex, strongly continuous in $\{v \in W^{1,p}(\Omega), v \geq 0\}$ and then lower-semi-continuous [**JB**]. However, since $h_{n+\frac{1}{2}}$ is not uniformly lower-bounded, coerciveness and thus well-posedness of the minimisation problem are not guaranteed.

3.2. Discretization in space. Let $M > 0$ be given, and suppose $\Omega = [x_0, ..., x_{M+1}]$ is a multilevel discretization that results from several successive local or global refinements applied to the initial interval $[x_0, x_{M+1}]$. Such a hierarchy is necessary to apply the Newton multigrid method which is used to solve the two minimisation problems (Steps I and III above). The transport problem (Step II) is solved using an upwind finite difference scheme.

The Ritz-Galerkin approximation of both of the minimization problems, in the standard continuous piecewise-linear finite element space, can be written

$$\text{find} \quad \mathbf{u} \in \mathbb{R}^I \quad \text{s.t.} \qquad \mathcal{J}(\mathbf{u}) \leq \mathcal{J}(\mathbf{v}), \qquad \forall \mathbf{v} \in \mathbb{R}^I, \tag{3.1}$$

where $I \in \mathbb{N}$. Here $\mathcal{J} : \mathbb{R}^I \longrightarrow \mathbb{R} \cup \{+\infty\}$ is a strictly convex, coercive, lower semi-continuous, but not necessarily smooth, nonlinear functional. Indeed, the obstacle in (2.4) and the case $m = 0$ in (2.9) lead to different nonsmooth terms in $\mathcal{J}_{SIA}$ and $\mathcal{J}_{SSA}$, respectively. Also, $\mathcal{J}_{SIA}$ and $\mathcal{J}_{SSA}$ are coercive in the finite dimensional spaces since all norms are equivalent.

Since Newton-type methods require smoothness, we use a truncated method, closely-related to the primal dual active set approach [**Kor94, Kor96, GK09**], to solve problems (3.1). Following the techniques that have been developed in [**GK09, GSS09, Grä11**] for linear and nonlinear obstacle problems, we use the Truncated Nonsmooth Newton MultiGrid (TNMMG) method, described next. By contrast, in [**Sch06a**] a regularisation parameter was introduced to deal with nonsmoothness for the approximation of the SSA when $m = 0$. Unfortunately, this approach might slow down the algebraic solver if the regularisation parameter is too small, or it might lead to a wrong solution if the parameter is too large.

Let $\mathcal{F} : \mathbb{R}^I \to \mathbb{R}^I$ be a nonlinear Gauß-Seidel smoother. More precisely, for a given iterate $\mathbf{u} \in \mathbb{R}^I$, $\mathcal{F}(\mathbf{u})$ provides the correction such the new iterate $\mathbf{u} + \mathcal{F}(\mathbf{u})$ minimizes successively $\mathcal{J}$ in each coordinate direction. Each scalar minimisation can be achieved by an inexact method. In practise, we use a bisection method since it does not require any smoothness. The TNNMG method [**Grä11**] then defines a sequence $\mathbf{u}^\nu$ by the following three steps per iteration:

$$\mathbf{u}^{\nu+\frac{1}{3}} = \mathbf{u}^\nu + \mathcal{F}(\mathbf{u}^\nu), \tag{3.2}$$

$$\mathbf{u}^{\nu+\frac{2}{3}} = \mathbf{u}^{\nu+\frac{1}{3}} - (\mathcal{J}''(\mathbf{u}^{\nu+\frac{1}{3}})_{\mathcal{I},\mathcal{I}})^{-1}\mathcal{J}'(\mathbf{u}^{\nu+\frac{1}{3}})_{\mathcal{I}}, \tag{3.3}$$

$$\mathbf{u}^{\nu+1} = \operatorname{argmin}_{\mathbf{w},\, \rho\in[0,1]}\{\mathcal{J}(\mathbf{w}); \quad \mathbf{w} = \rho\mathbf{u}^{\nu+\frac{1}{3}} + (1-\rho)\mathcal{P}_{Dom(\mathcal{J})}(\mathbf{u}^{\nu+\frac{2}{3}})\} \tag{3.4}$$

where the active index set is denoted

$$\mathcal{I} = \mathcal{I}(\mathbf{v}) = \{i, \text{ the subdifferential } \partial\mathcal{J}(v_i) \text{ is single-valued}\}. \tag{3.5}$$

Here $(\cdot)_{\mathcal{I}}$ and $(\cdot)_{\mathcal{I},\mathcal{I}}$ denote the truncation of vectors and matrices, respectively, to the index set $\mathcal{I}$; i.e. the i-th entry (and also the i-th column in the matrix case) is set to zero if i is not in $\mathcal{I}$. Also, $\mathcal{P}_{Dom(\mathcal{J})}$ denotes the projection onto the convex set $Dom(\mathcal{J}) = \{\mathbf{u}, \mathcal{J}(\mathbf{u}) < +\infty\}$.

Step (3.2) acts as a smoother of all nonlinearities. In particular, this step allows the set of active nodes $\mathcal{I}(\mathbf{v})$ to be modified. Step (3.3) consists of a Newton correction that applies in the smooth coordinate directions only. The set of active nodes $\mathcal{I}(\mathbf{v})$ is fixed during this step. Since the matrix $\mathcal{J}''(\mathbf{u}^{\nu+\frac{1}{2}})_{\mathcal{I},\mathcal{I}}$ is symmetric and positive definite on the subspace $\{\mathbf{u} \in \mathbb{R}^I, u_i = 0 \text{ if } i \notin \mathcal{I}(v)\}$ we apply a linear multigrid method for the inversion of $\mathcal{J}''(\mathbf{u}^{\nu+\frac{1}{2}})_{\mathcal{I},\mathcal{I}}$. More precisely, we implement a V-cycle type multigrid solver combined with a linear Gauß-Seidel smoother with 3 pre- and post-smoothing steps [**Hac85**]. Since the Newton correction (3.3) might act beyond the convex set $Dom(\mathcal{J})$, the third projection step (3.4) is constrains the Newton correction to remain in $Dom(\mathcal{J})$. Since the projected correction is not assured to have a lower energy than $\mathbf{u}^{\nu+\frac{1}{3}}$, a damping parameter ρ guarantees the monotonicity and the global convergence of the method [**Grä11**].

The implementation is based on the code *DUNE* (http://www.dune-project.org/) and its module *Dune-Tnnmg* [**GSS09**].

4. Numerical results

We consider the polynomial bedrock over the domain $\Omega = [-1000, 1000]$ km shown in Fig. 2. We initialize the ice geometry by a ten meter thick layer of ice (grounded and floating) on Ω and we apply a constant-in-time mass balance defined $a(x) = -1$ m y^{-1} if $x < -500$ km and $a = 0.3$ m y^{-1} elsewhere. We run our model until reaching a steady state shape. On the left-hand-side of the domain Ω, the chosen mass balance with an ablation area allows a free grounded margin to form, while there is an ice-water cliff on the right boundary of Ω. We use of the following parameters: $\rho_i = 900$ kg m^{-3}, $\rho_w = 1000$ kg m^{-3}, $g = 9.81$ m s^{-2} and $A = 4.6416 \times 10^{-24}$ Pa^{-3} s^{-1}. Two experiments are performed using different sliding parameterizations: (**a**) $m = 1/3$ and $C = 7.624 \times 10^6$ Pa m$^{-1/3}$ s$^{1/3}$ and (**b**) $m = 0$ and $C = 10^5$ Pa. Experiment (**a**) involves a power-type sliding law like in [**Sch07, PSP$^+$12**] while experiment (**b**) involves a Coulomb-type law [**Sch06b, Sch09**].

The domain Ω is uniformly meshed at a resolution of ~ 15 km and adaptively refined 5 km around the grounding line to a resolution of ~ 0.1 km in order to capture the high gradients of the solution expected in this area [**PSP$^+$12**]. Since we use an upwind finite difference scheme to solve the mass conservation equation, each time step is updated such that the CFL number never exceeds one. In practise, we start with a time step of 5 years, however, this time step decreases as low as ~ 0.1 year because of this stability criterion.

Fig. 2 displays the steady state shapes of our model with the corresponding SIA and SSA velocities for both sliding parameterizations. Both shapes were found after $\sim 10\,000$ years. The results lead to the following physical observations. First, as expected the SIA velocities are dominant in the ice sheet part while the SSA velocities are much larger in the ice shelf area for both sliding parameterizations. Second, power-law-type sliding allows SSA velocities to be nonzero everywhere, while Coulomb-type sliding allows nonzero SSA velocities only in the transition and floating areas. Third, the power-type sliding law induces a steeper gradient in surface elevation at the grounding line position compared to the Coulomb-type law. This geometric difference arises because, in the power law case, the basal shear stress can rise with increasing sliding velocity as the grounding line is approached from the grounded side, so as to balance higher driving stress from a steeper surface gradient. In the Coulomb case, by contrast, the basal stress is limited to the prescribed yield stress (i.e. $C = 10^5$ Pa in experiment (**b**)).

From a numerical point of view, the TNNMG method turns out to be a valuable tool to solve the two minimisation problems related to the SIA and the SSA. Indeed, Newton-type methods do not directly apply since $\mathcal{J}_{SIA}$ is nonsmooth because of the obstacle while $\mathcal{J}_{SSA}$ is nonsmooth in the $m = 0$ (Coulomb sliding) case. The TNNMG method based on truncation is expected to be faster than a classical regularized solver [**Sch06b**] since the truncated system in (3.3) is smaller, and an experimental comparison in the $m = 0$ case shows that TNMMG is $\sim 12\%$ faster compared to a Newton multigrid method with regularized nonsmooth parts. Of course, TNNMG does not depend on arbitrary regularisation parameters. Note that the TNNMG method converges quadratically in the iterations (3.2)-(3.4) and

linearly when skipping the Newton correction (3.3), i.e. when applying a single Gauß-Seidel method. For instance, in our example the TNNMG method used only 13 iterations were needed against more than 500 for a single Gauß-Seidel method to compute one SSA velocity field with the same accuracy. It took around 10 minutes (CPU time) on a single 3.30GHz processor to compute the 15 000 time steps necessary to reach the steady state shape of the experiment (**b**). The CPU times for minimizing $\mathcal{J}_{SIA}$ and $\mathcal{J}_{SSA}$ were comparable while the time to compute the advection problem (Step II) was negligible.

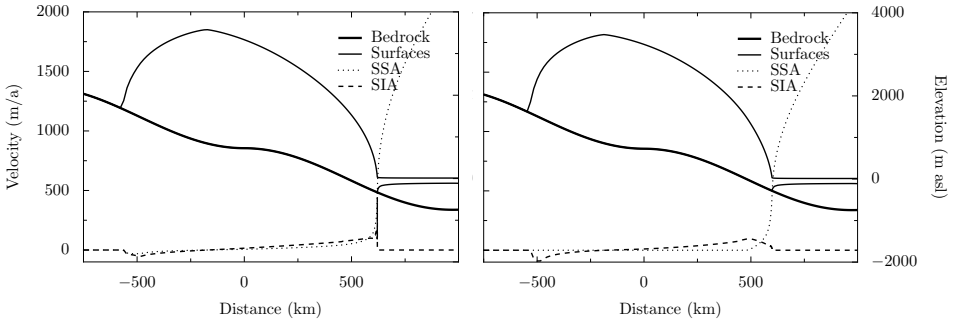

FIGURE 2. Steady state shapes of a two-dimensional idealized system ice sheet/shelf for (**a**; left) a power-type sliding law (**b**; right) a Coulomb-type sliding law. SIA and SSA velocities are displayed with dashed and dotted lines, respectively.

Combining a Newton correction, a truncation procedure to treat nonsmoothness, and a linear multigrid solver provides a fast and robust solver for variational inequality problems (2.4) and (2.9). The TNNMG method can be easily extended to three-dimensional ice sheet and ice shelf models. However, grid refinements around the grounding line, and numerical techniques to solve the mass conservation equation, require more attention. These issues will be addressed in future work.

References

[BB09] E. Bueler and J. Brown, *Shallow shelf approximation as a "sliding law" in a thermomechanically coupled ice sheet model*, Journal of Geophysical Research - Earth Surface **114** (2009), no. F3, F03008+.

[CDD+02] N. Calvo, J. I. Díaz, J. Durany, E. Schiavi, and C. Vázquez, *On a doubly nonlinear parabolic obstacle problem modelling ice sheet dynamics*, SIAM Journal on Applied Mathematics **63** (2002), no. 2, 683–707 (electronic). MR MR1951955 (2004g:86019)

[DGDF+09] G. Durand, O. Gagliardini, B. De Fleurian, T. Zwinger, and E. Le Meur, *Marine ice sheet dynamics: Hysteresis and neutral equilibrium*, Journal of Geophysical Research **114** (2009).

[DPF11] D. Docquier, L. Perichon, and Pattyn F., *Representing grounding line dynamics in numerical ice sheet models: Recent advances and outlook*, Surveys in Geophysics **32** (2011), 417–435.

[GB09] R. Greve and H. Blatter, *Dynamics of ice sheets and glaciers*, Springer Verlag, 2009.

[GHS09] D. Goldberg, D. M. Holland, and C. Schoof, *Grounding line movement and ice shelf buttressing in marine ice sheets*, Journal of Geophysical Research **114** (2009), no. F04026.

[GK09] C. Gräser and R. Kornhuber, *Multigrid methods for obstacle problems*, Journal of Computational Mathematics **27** (2009), no. 1, 1–44.

[Glo03] R. Glowinski, *Handbook of numerical analysis: Numerical methods for fluids (part 3)*, vol. 9, Elsevier Science Ltd, 2003.

[Grä11] C. Gräser, *Convex minimization and phase field models*, Ph.D. thesis, FU Berlin, 2011.

[GSS09] C. Gräser, U. Sack, and O. Sander, *Truncated nonsmooth newton multigrid methods for convex minimization problems*, Domain Decomposition Methods in Science and Engineering XVIII, Lecture Notes in Computational Science and Engineering, vol. 70, Springer Berlin Heidelberg, 2009, pp. 129–136.

[Hac85] W. Hackbusch, *Multi-grid methods and applications*, Springer series in computational mathematics, Springer, 1985.

[JB] G. Jouvet and E. Bueler, *Steady, shallow ice sheets as obstacle problems: well-posedness and finite element approximation*, SIAM Journal on Applied Mathematics, accepted for publication.

[Kor94] R. Kornhuber, *Monotone multigrid methods for elliptic variational inequalities. I*, Numerische Mathematik **69** (1994), no. 2, 167–184.

[Kor96] R. Kornhuber, *Monotone multigrid methods for elliptic variational inequalities. II*, Numerische Mathematik **72** (1996), no. 4, 481–499.

[PHDBDS06] F. Pattyn, A. Huyghe, S. De Brabander, and B. De Smedt, *Role of transition zones in marine ice sheet dynamics*, Journal of Geophysical Research **111** (2006), no. F2, 1–10.

[PSP+12] F. Pattyn, C. Schoof, L. Perichon, R. C. A. Hindmarsh, E. Bueler, B. de Fleurian, G. Durand, O. Gagliardini, R. Gladstone, D. Goldberg, G. H. Gudmundsson, V. Lee, F. M. Nick, A. J. Payne, D. Pollard, O. Rybak, F. Saito, and A. Vieli, *Results of the marine ice sheet model intercomparison project, MISMIP*, The Cryosphere Discussions **6** (2012), no. 1, 267–308.

[Sch06a] C. Schoof, *A variational approach to ice stream flow*, Journal of Fluid Mechanics **556** (2006), 227–251.

[Sch06b] C. Schoof, *Variational methods for glacier flow over plastic till*, Journal of Fluid Mechanics **555** (2006), 299–320.

[Sch07] C. Schoof, *Ice sheet grounding line dynamics: Steady states, stability, and hysteresis*, Journal of Geophysical Research **112** (2007).

[Sch09] C. Schoof, *Coulomb friction and other sliding laws in a higher order glacier flow model*, Mathematical Models and Methods in Applied Sciences (2009).

[Sch11] C. Schoof, *Marine ice sheet dynamics. Part 2: A stokes flow contact problem*, Journal of Fluid Mechanics **679** (2011), 122–155.

[VA07] D. G. Vaughan and R. Arthern, *Why is it hard to predict the future of ice sheets ?*, Science **315** (2007), no. 5818, 1503–1504.

[VP05] A. Vieli and A. J. Payne, *Assessing the ability of numerical ice sheet models to simulate grounding line migration*, Journal of Geophysical Research **110** (2005), no. F1, 1–18.

[WMH+11] R. Winkelmann, M. A. Martin, M. Haseloff, T. Albrecht, E. Bueler, C. Khroulev, and A. Levermann, *The Potsdam Parallel Ice Sheet Model (PISM-PIK) Part 1: Model description*, The Cryosphere **5** (2011), 715–726.

Institut für Mathematik, Freie Universität Berlin, Berlin, Germany
E-mail address: guillaume.jouvet@fu-berlin.de

Department of Mathematics and Statistics, and Geophysical Institute, University of Alaska Fairbanks, USA
E-mail address: elbueler@alaska.edu

Institut für Mathematik, Freie Universität Berlin, Berlin, Germany
E-mail address: graeser@math.fu-berlin.de

Institut für Mathematik, Freie Universität Berlin, Berlin, Germany
E-mail address: ralf.kornhuber@fu-berlin.de